Nuclear Instruments and Methods in Physics Research B 544 (2023) 165123

Contents lists available at ScienceDirect

Nuclear Inst. and Methods in Physics Research, B

journal homepage: www.elsevier.com/locate/nimb

On the missing single collision peak in low energy heavy ion scattering

R.A. Wilhelm [a,*], M.J. Deuzeman [b,c], S. Rai [b,c], W. Husinsky [a], P.S. Szabo [d], H. Biber [a], R. Stadlmayr [a,e], C. Cupak [a], J. Hundsbichler [f], C. Lemell [f], W. Möller [g], A. Mutzke [h], G. Hobler [i], O.O. Versolato [c,j], F. Aumayr [a], R. Hoekstra [b,c]

[a] TU Wien, Institute of Applied Physics, Wiedner Hauptstr. 8-10/E134, 1040 Vienna, Austria
[b] Zernike Institute for Advanced Materials, University of Groningen, Nijenborgh 4, 9747 AG Groningen, The Netherlands
[c] Advanced Research Center for Nanolithography (ARCNL), Science Park 106, 1098 XG Amsterdam, The Netherlands
[d] University of California, Space Sciences Laboratory, 7 Gauss Way, Berkeley, CA 94720, United States of America
[e] Berndorf Band GmbH, Leobersdorfer Str. 26, 2560 Berndorf, Austria
[f] TU Wien, Institute for Theoretical Physics, Wiedner Hauptstr. 8-10/E134, 1040 Vienna, Austria
[g] Helmholtz-Zentrum Dresden-Rossendorf, Institute of Ion Beam Physics and Materials Research, Bautzner Landstr. 400, 01328 Dresden, Germany
[h] Max Planck Institute for Plasma Physics, Wendelsteinstr. 1, 17491 Greifswald, Germany
[i] TU Wien, Institute of Solid-State Electronics, Gußhausstraße 25-25a, 1040 Vienna, Austria
[j] Department of Physics and Astronomy, and LaserLaB, Vrije Universiteit, De Boelelaan 1081, 1081 HV Amsterdam, The Netherlands

ARTICLE INFO

Keywords:
Heavy ions
Ion scattering
Molecular dynamics
Binary collision approximation

ABSTRACT

We present experimental and simulation data on the oblique angle scattering of heavy Sn ions at 14 keV energy from a Mo surface. The simulations are performed with the binary collision approximation codes TRIM, TRIDYN, TRI3DYN, SDTrimSP, and IMSIL. Additional simulations were performed in the molecular dynamics framework with LAMMPS. Our key finding is the absence of an expected peak in the experimental energy spectrum of backscattered Sn ions associated with the pure single collision regime. In sharp contrast to this, however, all simulation codes we applied do show a prominent single collision signature both in the energy spectrum and in the angular scatter pattern. We discuss the possible origin of this important discrepancy and show in the process, that widely used binary collision approximation codes may contain hidden parameters important to know and to understand.

1. Introduction

The interaction of heavy ions in the keV energy range with material surfaces has important scientific and industrial applications in surface polishing, cleaning, milling, and nanostructuring in general. All these types of material modifications are initiated by momentum transfer of the ions to the lattice atoms. A collisional cascade evolves and the part which reaches and escapes from the surface determines the ion's sputtering yield.

At (near) normal incidence angles, the primary ion is likely to be implanted in the material or, depending on surface chemistry, it may diffuse outwards again. Still, its entire initial momentum is transferred to the material. At off-normal incidence, however, the ion can be reflected from the surface by single collisions or as a result of multiple collisions in the near-surface region. While the ion backscattering at low energies is used in analysis methods such as low energy ion scattering (LEIS) utilizing light ions, like H and He, there is only little body of literature on slow heavy ion backscattering so far. A reduced large-angle backscattering cross section and a severe energy broadening due to multiple scattering hamper the application of slow heavy ions in surface analysis. Also the atomic-scale modelling of the full chain of collision processes is highly challenging in realistic molecular dynamics simulations.

Despite, there exist industrial applications where a deep understanding of heavy ion scattering is important to quantify material changes and degradation under slow heavy ion impact. In modern extreme ultraviolet (EUV) light lithography machines Sn plasmas are created at a rate of 50 kHz by exposing a stream of Sn droplets to intense laser pulses (Refs. [1–4] and references therein). Inside the plasma, singly, doubly, and triply excited Sn ions in charge states 8–14 are the atomic sources of the 13.5 nm EUV radiation [5]. Sn ions from the expanding plasma have kinetic energies in the keV regime with tails up to many tens of keV [6–9] and may reach sensitive devices facing the plasma, as for example the extremely highly polished EUV multilayer mirrors which consist typically of alternating thin Mo and Si layers [10]. The

* Corresponding author.
E-mail addresses: wilhelm@iap.tuwien.ac.at (R.A. Wilhelm), r.a.hoekstra@rug.nl (R. Hoekstra).

https://doi.org/10.1016/j.nimb.2023.165123
Received 13 April 2023; Received in revised form 18 September 2023; Accepted 18 September 2023
Available online 4 October 2023

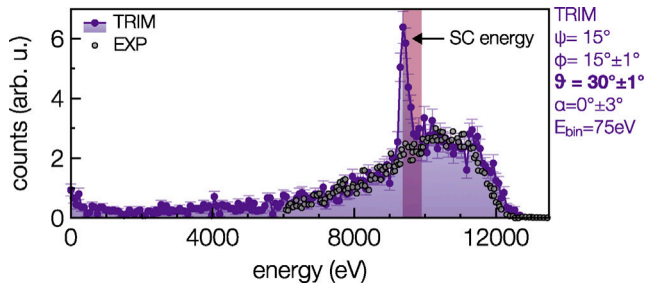

Fig. 1. Experimental and TRIM spectrum of 14 keV Sn^{1+} backscattered from a Mo surface. The definition of the angles is given in Fig. 2. The red shaded area indicates the expected energy range for the single collision (SC) peak, which is prominently present in the TRIM simulation, but completely absent in the experimental data.

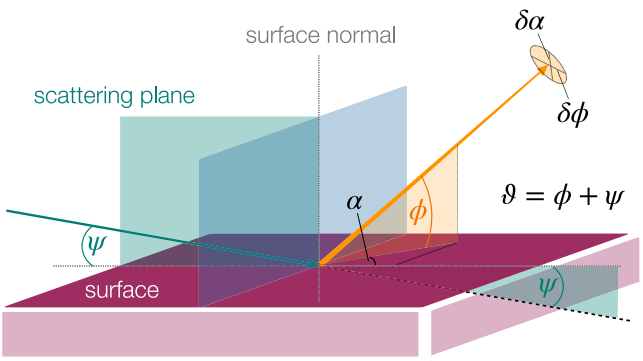

Fig. 2. Definition of angles. ψ is the incident angle with respect to the surface plane, ϕ is the exit angle wrt. the surface plane and $\vartheta = \psi + \phi$ is the scattering angle in the scattering plane. The angle α is the scattering angle out of the scattering plane (green) and $\delta\alpha$ as well as $\delta\phi$ are the angular ranges which are used to compare to experiment, i.e., the detector acceptance angles.

ions reach the surfaces at different angles and it becomes important to understand to which extent the impact of the ions leads to sputtering or other structural changes and whether the Sn ions are implanted or backscattered.

Here we investigate the backscattering of slow (14 keV) Sn ions from a Mo surface experimentally and by means of the widely used binary collision approximation (BCA) codes TRIM [11], as well as TRIDYN [12], TRI3DYN [13], SDTrimSP [14], and IMSIL [15]. We also applied molecular dynamics simulations using the LAMMPS code [16–18]. Fig. 1 introduces the main feature we want to discuss in this paper. At oblique angles of incidence it is expected that ions (a) penetrate the surface with a fraction subsequently being scattered out of the surface again (multiple scattering) or (b) are reflected from the surface by a single collision (SC) event. The experimental energy spectrum of Sn ions, however, shows no SC peak [19,20], whereas it is expected at around 9.5 keV for the given parameters in Fig. 1. TRIM, however, clearly shows the SC peak and fits the experiment perfectly otherwise. In this work we want to discuss possible origins for the drastic discrepancy between experiment and simulation for this fairly simple scattering system.

In the following, energy- and angle-dependent backscattering spectra are calculated with a strong focus on the SC peak, i.e., a peak in the energy spectrum (or a ridge in the energy-angle 2D spectrum) caused by Sn scattered only once from one of the topmost Mo atoms. As it turns out, comparisons between simulation and experiment are very sensitive to the exact experimental settings of detector acceptance angles, energy binning of spectra and overall detector positioning. Choosing a non-ideal set of parameters may obscure the SC peak. Further, we show that surface oxidation of Mo may change the spectrum drastically, whereas the surface roughness has only a small influence. We discuss that the absence of the SC peak in experiments might have at least two causes: charge exchange of the ions during scattering which is not considered explicitly in simulations and/or the (poly-)crystalline nature of the Mo surface always present in experiment and in our LAMMPS as well as IMSIL simulations, but completely neglected in the other BCA codes.

2. Experimental setup

The experiments were performed at ZERNIKELEIF facility at the University of Groningen and details are published in [19,20]. Let us only briefly describe the general setup. Sn ions are produced in an Electron Cyclotron Resonance (ECR) ion source and a 110° analysing magnet is used to select a beam of $^{120}Sn^{2+}$ ions. The beam is guided by means of magnetic quadrupole triplets through the central beam line of the facility and after 15 m bend out of the beam line and injected in the target chamber by means of a 45° dipole magnet. At the entrance of the collision chamber is a set of diaphragms which guarantees an angular spread of the beam of $< 1°$. The energy of the beam is 14 keV with an energy spread of about 15 eV. The rectangular ($8 \times 6\,mm^2$) polycrystalline Mo target was commercially acquired from Surface Preparation Labs (SPL, Zaandam, the Netherlands) and installed on a standard VG manipulator in the centre of a μ metal scattering chamber kept at a base pressure of $1 \cdot 10^{-8}$ mbar.

The angle of incidence was adjusted by means of the rotational target holder to an accuracy of better than 1°. Scattered ions are detected with a rotatable electrostatic analyser positioned at 30° and 45° in forward direction with respect to (wrt.) the incoming beam direction. At 40° to the incoming beam a time-of-flight spectrometer was mounted to detect also neutral particles. In this case the incoming beam was electrostatically chopped in order to provide a well-defined start signal.

3. Modelling setup

In the following sections we will use the angle definition, which is presented in Fig. 2. The angle ψ is defined as the angle of incidence with respect to the surface plane. Therefore, the incidence angle wrt. the surface normal is $90° - \psi$. Further, the outgoing angle wrt. the surface plane is ϕ. The scattering angle $\vartheta = \psi + \phi$ is used here only for the scattering plane, i.e., $\alpha = 0$. The ion can leave the surface at an angle α, which points out of the scattering plane. We will also use $\pm\delta\alpha$ and $\pm\delta\phi$, which are intervals around the mean exit angles $\{\alpha, \phi\}$ and it turns out, that these angular resolutions are important when comparing to an experiment, where finite values manifest as the detector acceptance angles.

All simulations shown below are for 14 keV Sn ions with the mass of 118.7 amu, i.e., the weighted mass of the natural isotope ratio. The surface consists of Mo_xO_y with $x = 0.25–1$ and $y = 0–0.75$ for different simulations (see Appendix). The Mo mass in the simulations is 95.94 amu, but it should be noted that Mo has stable (long-lived) isotopes ranging form 92–100 amu. The SC peak width (cf. Fig. 1) will have some additional broadening from the different isotopes in the Mo and we estimate this broadening to be about ~ 250 eV based on Eq. (1) below.

We use the BCA codes TRIM (part of the SRIM 2013 package), SDTrimSP 6.01, TRIDYN 2022, TRI3DYN, IMSIL as well as the molecular dynamics code LAMMPS. Further details are given in the subsections below. All spectra are scaled arbitrarily in order to compare different features between codes.

3.1. Binary collision approximation

3.1.1. TRIM

We use the TRIM code with the 'Damage detail' set to 'Detailed Calculation with full Damage Cascades'. The ion and target are set as

described above. We analysed the output file for the backscattered ions wrt. the ion energy and exit angles. Each simulation is run until at least 500,000 ions are backscattered.

3.1.2. TRIDYN

We used the TRIDYN code in the version 2022 in the static mode. With this one-dimensional code we simulated the spectrum for the respective ion energy and angles using standard parameters (KrC screening potential). We further investigated the influence of the surface binding energy of the Sn ion and set it to zero, because a non-zero value may cause a deflection (of the ion) when crossing the surface layer from/to vacuum. We also changed the thickness of an artificially introduced above-surface-layer (ASL) in the code of initial (default) thickness $2\varrho^{-1/3}/(\sqrt{\pi})$ (ϱ is the atomic density of the material), which is introduced to describe scattering effects close-to, but outside of the surface. We further checked the influence of 'soft scattering'. Soft scattering is implemented in most BCA codes originating from TRIM (i.e., also the ones used here except for IMSIL), where for each true scattering event along the mean free path of $\varrho^{-1/3}$, a number of additional scattering events is calculated with a distance larger than $\varrho^{-1/3}$. Soft scattering is intended to mimic the multi-particle interaction with atoms at larger distances, similarly to the fully many body description in Molecular Dynamics.

3.1.3. TRI3DYN

In TRI3DYN we used only the static mode, e.g., did not account for a changing target composition or shape, with standard parameters (especially the KrC screening potential and pre-defined surface binding energies). The code allows us to use a rough surface and we generated a random surface with a given root mean square (RMS) roughness, see Appendix. The surface is mirrored in two directions in order to use periodic boundary conditions in both surface directions. We further considered different oxidation states of the Mo surface by setting a specific stoichiometry (see Appendix). TRI3DYN also allows us to extract the number of collisions for each backscattered ion. We considered the incoming beam with a radial-symmetric Gaussian angular profile and varied the full-width-at-half-maximum (FWHM) of this 2D-angular distribution to mimic a finite emittance of the beam in the experiment (see Appendix).

The output file for the backscattered ions in TRI3DYN contains the energy information with 5-digit precision and the exponent, i.e., for an ion between 1.0 and 10 keV the precision is 1 eV (e.g., 0.1779E+04 eV). This pre-defined binning of the energy output leads, together with the re-binning for decreasing the statistical errors, e.g., to 80 eV (c.f. Fig. 16(d)), to an oscillation of the histogram. It should be noted that this is an artefact of the representation and in principle for more calculated ion trajectories the post-binning to 80 eV is not necessary. Note, that TRI3DYN treats the surface differently than TRIDYN (and other 1-dimensional BCA codes), i.e., no ASL exists in TRI3DYN.

3.1.4. SDTrimSP

We checked the results of TRI3DYN (see Appendix) with SDTrimSP using mostly the same input parameters, where both codes are in good agreement. We also checked the effect of the surface oxidation again with SDTrimSP by setting different stoichiometries (see Appendix). SDTrimSP uses the KrC screening function by default, and we also changed it to the ZBL screening function as this is used in TRIM (see Appendix). For the numerical method for the scattering angle determination we used both the standard Gauss–Legendre quadrature and the Magic formula, respectively.

3.1.5. IMSIL

We used the IMSIL code developed at TU Wien with standard parameters. The code allows, in addition to a random mode as implemented in other BCA codes, a BCA-type modelling of (poly-)crystalline targets, i.e., impact parameters and scattering partners are not randomly selected, but according to a pre-defined lattice. We implemented the Mo bcc lattice as a single crystal with (001) surface orientation. We further prepared a polycrystalline Mo target by randomly rotating the crystal before each ion impact, and an amorphous target, whereas the latter should be comparable to the simulation outputs of SDTrimSP, TRIDYN and TRI3DYN in the latter scenario. The single crystalline case should be comparable to the simulations using LAMMPS (see below). In contrast to the other BCA codes, a maximum impact parameter of 3 Å is chosen in order to always include "soft scattering". In the crystalline mode lattice vibrations corresponding to a lattice temperature of 300 K are considered.

3.2. Molecular dynamics

Molecular Dynamics (MD) simulations were performed with the LAMMPS (Large-scale Atomic/Molecular Massively Parallel Simulator) code [16–18]. The computations were performed on the Vienna Scientific Cluster (VSC).

The Mo target consists of approximately 110 000 atoms in the central cell with periodic boundary conditions employed. This size was kept low to make the simulation of one ion trajectory not too computationally expensive, but large enough to keep the damage of the crystal limited to a fraction of the total crystal size and keep the influence on the scattered ions negligible. For the simulations a MEAM/spline (Modified Embedded-Atom Method) potential was used for the Mo atoms and a ZBL potential between the Sn and Mo atoms.

Before simulating the Sn ion trajectory, the target was brought into thermal equilibrium at 1900 K. In addition, the thermalization process time was set to $t + \Delta t$ with Δt chosen randomly for each simulation run, assuring slightly different crystal atom positions for each run. The high temperature was chosen to randomize the Mo atom positions in order to mimic a (moderate) disorder of the crystal and compare to the BCA codes.

Simulations have been performed for $\psi = 5$, 10, 15, and 25° as well as 14 and 25 keV (not shown). The ion impact location at the surface was varied randomly within the distance of a unit cell of the Mo target for each simulation run. The individual ions started about 15 atomic layers above the surface and 20 atomic layers to the left of the target. The MD simulation runs long enough to ensure that the scattered Sn ion has left the surface (500 fs). In addition, this time has also been chosen to be able to detect some promptly sputtered atoms. But in order to achieve a reasonable statistic, the time was not sufficient to detect most sputtered particles, which would have required 20 ps or even more. Since the sputtered atoms have typically energies in the 10 eV range, they do not contribute to the energy region of the SC peak we want to investigate. The information of all atoms (scattered and sputtered) detected above the surface have been stored for further data analysis (see chapters below): energy, spatial info (see Fig. 2) and closest distance to the target surface for the Sn ion on its path.

The major challenge of the MD simulations of the ion scattering process is to obtain reasonable statistics. To perform a sufficient number of individual simulations we employed a high-performance computing platform of the VSC. SLURM array jobs consisting of 100 members in the job array were set up each using single computing nodes and the associated 48 cores available on them for parallel MD runs on single cores. Under perfectly ideal conditions, this would result in 4800 MD simulations running in parallel. In practice, however, individual nodes will become available only in smaller quantities over time. Hence, the results presented here consumed approximately 100 days of computing time. The total number of scattered ions obtained was around 2.5×10^6 for 15° incoming angle and close to 1×10^6 for most other angles of incidence.

3.3. Simplified molecular dynamics

For low incident angles the scattering at a given atom i can be influenced by the deflection due to the force fields of the $(i-1)$-th atom along the ion trajectory above the surface. Therefore, the scattering event depends on the particular history of the incoming ion. The deflection before the main scattering event leads to a change in impact parameter and therefore a change in incident and scattering angle. We will call this effect of a changing incoming trajectory due to the previously encountered target atoms 'soft multi-scattering' in the following. Note the difference to conventional multiple scattering, which is a sequence of scattering events without spatial correlation between individual events. To evaluate the importance of soft multi-scattering, we performed a simplified MD calculation. We positioned a single Mo atom at the surface and considered different impact parameters, see. Fig. 7(a). We repeated the same calculation adding 6 additional atoms along one dimension and see that different impact parameters can now result in the same scattering angle (cf. Fig. 7(b)). Here we only consider the forces between the ion and the target atoms given by the gradient of the ZBL potential. The target atoms are pinned and grid forces are not considered. Finally we prepared a two-dimensional cubic lattice of atoms and followed the trajectories for random impact positions within the central unit cell.

4. Results and discussion

In the following Section 4.1–4.10 we elaborate on results on specific numerical calculations methods, their possible artefacts and limitations. We emphasize the importance of individual features like surface oxidation, roughness or crystallinity in a comparison with experimental data. In 4.11 we will then compare selected simulation results to the actual experimental data.

4.1. TRIM

The TRIM result shown in Fig. 3(a) presents the energy and out-of-plane exit angle of the Sn ions, with the highest intensity at high energies around $\phi = \psi = 10°$. We highlight the calculated SC peak energy from

$$E_{SC} = E_{kin}\left(\frac{m_{Sn}}{m_{Sn}+m_{Mo}}\right)^2 \times \left(\cos(\phi+\psi) \pm \sqrt{\frac{m_{Mo}^2}{m_{Sn}^2} - \sin(\phi+\psi)^2}\right)^2 \quad (1)$$

with m_{Sn} and m_{Mo} as the masses of Sn and Mo, respectively and the initial kinetic energy of $E_{kin} = 14$ keV. It can be seen in the TRIM results as a ridge of higher intensity ranging slightly below the calculated value.

The energy-width of the ridge in TRIM results from large impact parameter secondary collisions where some small energy loss occurs either on the way in or the way out. Energies higher and lower than the SC energy result from multiple collisions and they do not show any clear angular pattern. Noticeable is a jump in intensity exactly at $\psi = \phi = \vartheta/2$ (cf. inset in Fig. 3). For angles slightly below ψ, the SC peak is only weak in intensity compared to the multiple collision background (cf. Fig. 3(b)). At $\phi \geq \psi$ the SC peak becomes clearly visible both in the 2D spectrum (a) and in the projected spectra (c) and (d). Note that the width and intensity of the SC peak in (b) and (c) is strongly influenced by the energy binning used and the choice of $\delta\alpha$ and $\delta\phi$. The intensity jump at $\phi = \psi$ seems nonphysical. We expect the value for $\phi < \psi$ to be significantly underestimated in TRIM as an artefact of how ion trajectories are evaluated for shallow scattering angles, i.e., $\vartheta < 2\psi$, cf. [20]. Unfortunately, TRIM does not allow to track the collision details particularly for backscattered ions. The labelling of ions in the backscattering output file is different from the ions in the collisional

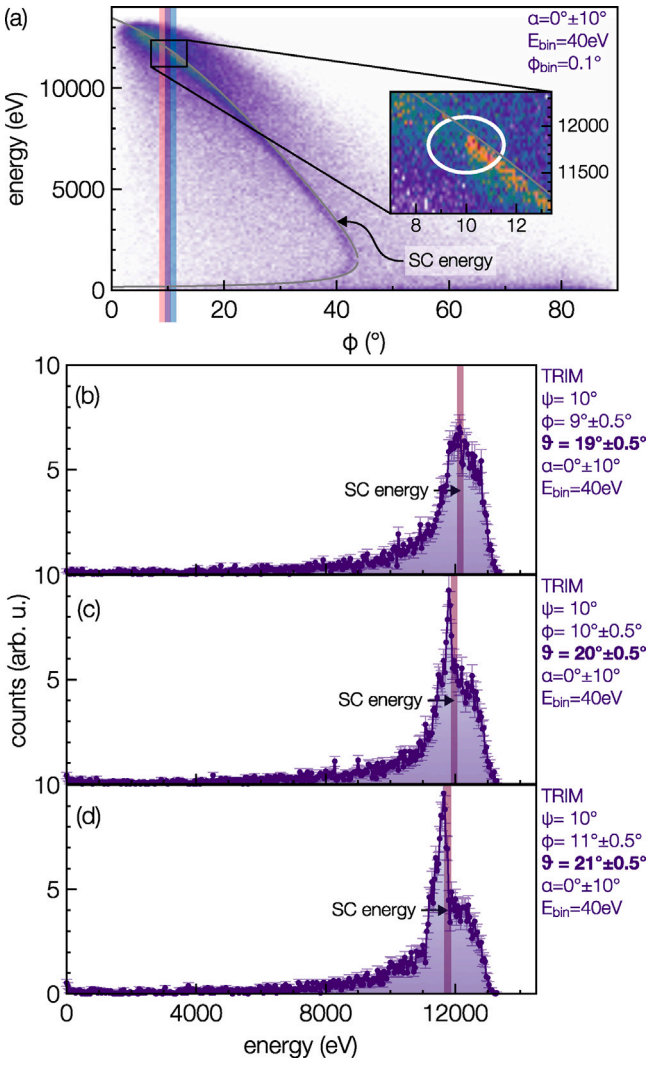

Fig. 3. TRIM result for 14 keV Sn on Mo for $\psi = 10°$. In the two-dimensional energy-ϕ histogram one can see a jump in intensity at $\psi = \phi$ (see inset in (a)). (b)–(d) are the projected energy spectra for $\phi = \psi - 1°$, $\phi = \psi$, and $\phi = \psi + 1°$ (coloured areas in (a)), respectively, where angular widths of $\delta\phi = 0.5°$ and $\delta\alpha = 10°$ are used for reasonable statistics. The grey line is the SC energy according to Eq. (1).

detail output file. The latter, however, does not contain any angular information. As a consequence, we can only guess where the issue at $\phi = \psi$ arises. For shallow scattering angles the outgoing part of the trajectory is closer to the surface than the incoming part, while this turns around at the critical angle. We assume that, TRIM introduces another scattering event above the surface which causes the ion to alter its direction of motion and to lose energy. Therefore, the SC peak is smeared out both in angle and in energy. TRIM calculates a scattering event choosing a random impact parameter and azimuthal angle after a mean free path of $\varrho^{-1/3}$. For our Mo target the scattering mean free path amounts to 2.6 Å, which means for scattering at the surface plane and at $\phi = \psi$ the ion would experience a second scattering event on the way out within a distance of 0.45 Å normal to the surface. For these small values it may seem plausible, that TRIM indeed considers this second scattering event even though it is outside the surface plane. It further implies that for $\phi > \psi$ this second scattering would be explicitly removed from the trajectory calculation. In light of this discussion, it is important to notice, that TRIM does not consider 'the way into the surface', i.e., the ion practically starts at the surface plane. Therefore, an above-surface-scattering artefact may only arise on the way out.

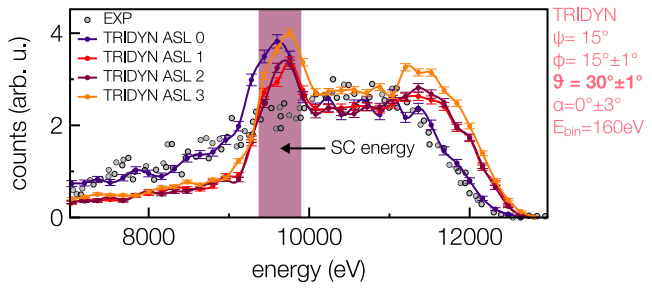

Fig. 4. TRIDYN simulations for 14 keV Sn on Mo with different thicknesses of an ASL. For a vanishing ASL, the overall spectral shape of the experiment is well reproduced (same as TRI3DYN and TRIM, cf. Fig. 12), but for non-zero ASL, the high energy edge is over- and the low energy tail is underestimated (same as IMSIL and SDTrimSP, not shown). The SC peak is generally missing in the experimental data.

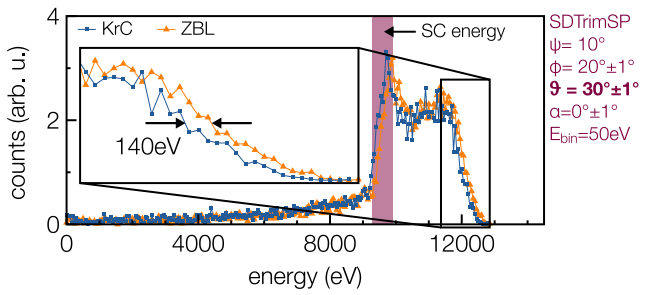

Fig. 5. SDTrimSP simulation for KrC and ZBL screening functions for 14 keV Sn on Mo.

4.2. Above-surface-layer (TRIDYN)

Regarding TRIDYN, the value of the surface binding energy showed no effect on the calculated spectrum of the ions. We used TRIDYN also to investigate the importance of an ASL. We changed the thickness of the ASL in integers of 0, 1, 2 and 3 times the initial thickness. The effect of the ASL is shown in Fig. 4, where also the precise parameters (angles and binning) are listed.

With any ASL the high energy edge (> 11.5 keV) is overestimated and the low energy edge (< 9 keV) is underestimated compared to the experimental data in this particular case. Without an ASL, the high and low energy edges from the experimental data are well reproduced. We therefore conclude, that the ASL should not be used when describing backscattered ions. The ASL, however, has no significant influence on the SC peak, which is generally not observed in the experimental data.

We also checked the influence of 'soft scattering' and found no significant influence on the energy spectrum. Soft scattering in the BCA models does change the energy, but no influence on the trajectory is considered, i.e., calculated and randomly chosen scattering angles (polar and azimuthal) are not changed by soft scattering. Typically the convention is that one soft scattering event per true scattering event is performed in BCA codes [21].

4.3. Screening function (SDTrimSP)

Fig. 5 shows the energy spectra for the different screening functions, $\psi = 10°$ and $\phi = 20°$. The change between KrC and ZBL screening affects the high energy edge of the spectrum. Since this edge results from small angle multiple scattering, the details of the screening function at large distances (large impact parameters, respectively) are more important than in the low energy part of the spectrum. The KrC screening function has a larger value than the ZBL screening for large(r) distances (up to ~ 20 screening distances) which increases the scattering strength (less screening) for small angle scattering. Therefore, one should expect that an angular deflection out of the surface is more likely for KrC screening and multiple large impact parameter scattering, but at the same time the energy transfer per scattering event might be larger. The shift of the high energy edge amounts to about 140 eV for this particular set of ion parameters and angular observation, i.e., about 1% of the incident energy. Note that this difference caused by different screening functions is much smaller than a possible influence of an ASL (c.f. Section 4.2). The change of the numerical approach to the scattering integral does not seem to have an effect on the spectra (not shown).

4.4. Molecular dynamics

We performed LAMMPS simulations for the target at 10 and 1900 K for a frozen single crystal and a somewhat randomized atomic arrangement, respectively. Fig. 6 shows the energy-angle 2D histograms, the angular patterns and the projected energy spectra for both temperatures, 14 keV and $\psi = 15°$ ((a) and (b)). In (c)–(f) the angular patterns are shown for all backscattered ions ((c), (e)) and for backscattered ions at a particular energy window where the SC peak should appear ((d), (f)). The angular distributions for both temperatures show a distinct pattern, whereas this pattern is sharper for 10 K in comparison to 1900 K. The pattern originates from scattering on a regular lattice, which will be elaborated in detail in the next section. We conclude, that the high temperature preparation is not sufficient to fully mimic random atom positions. For the energy filtered angular maps in (d) and (f), one can see the SC 'peak' appearing as a circle (indicated by the dotted line) with the radius of 20°, whereas this radius is given by the selected energy window (see Eq. (1)). For 10 K the SC peak is sharper in the angular pattern than for 1900 K. The projected energy spectra in (g) show the same behaviour, i.e., the 10 K spectrum shows two sharp peaks, the 1900 K spectrum two broader peaks. In general, the SC peak is visible in both cases, whereas a second high energy peak is visible. In (a) and (b) the energy-angle spectrum shows this bimodal energy distribution as an ellipse in the energy-ϕ plane. In particular this ellipse is higher in energy than the expected SC energy from Eq. (1) and its boundaries are again more defined for 10 K than for 1900 K. To clarify the origin of these peculiar energy spectra, we performed a simplified MD calculation with our self-developed code.

4.5. Soft multi-scattering (Simplified Molecular Dynamics)

Fig. 7 shows the impact parameter to scattering angle relation for a single binary collision and for the case of soft multi-scattering. In the latter, different impact parameters can lead to the same outgoing angle and therefore we might expect that the strict energy-angle relation in Eq. (1) gets distorted.

In fact, as a result of soft multi-scattering, the SC ridge in the energy-angle histogram (cf. Fig. 3(a)) becomes a closed-loop as shown in Fig. 8 with an on-average higher energy than given by Eq. (1). This phenomenon explains the observed loop in the LAMMPS simulations and the dual-peak structure in the energy spectrum (cf. Fig. 6(a) and (g)). For different incoming trajectories, i.e., different directions wrt. the crystalline directions, the loop can have different sizes and forms. From LAMMPS we see that some averaging over atomic positions (high temperature) smears out the boundaries of the loop. Nevertheless, these simplified MD simulations demonstrate that soft multi-scattering is an important effect on the SC peak in small angle scattering and cannot be captured by BCA codes with random atom positions.

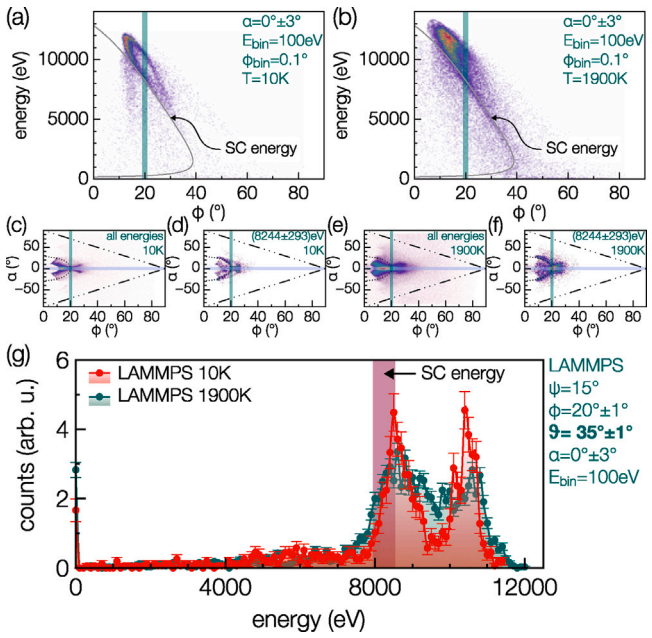

Fig. 6. LAMMPS results for 10 K and 1900 K of the Mo single crystal. Sn atoms at 14 keV have been simulated as projectiles with $\psi = 15°$. For higher temperatures the energy spectrum as well as angular pattern washes out. (a), (c), and (d) are for 10 K and (b), (e), and (f) for 1900 K.

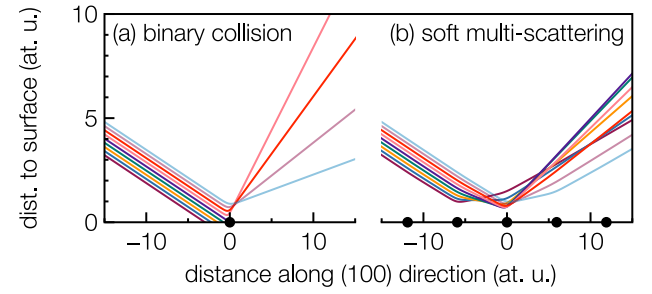

Fig. 7. Calculated scattering of 14 keV Sn ions on a single Mo atom at $(0, 0, 0)$ in (a) and a surface of Mo atoms located according to the bcc crystal positions in the x–y plane in (b). In (a) trajectories after scattering continue either in $-z$ or $+z$ direction (z being normal to the surface), while all trajectories point away from the surface in the case of soft multi-scattering (b).

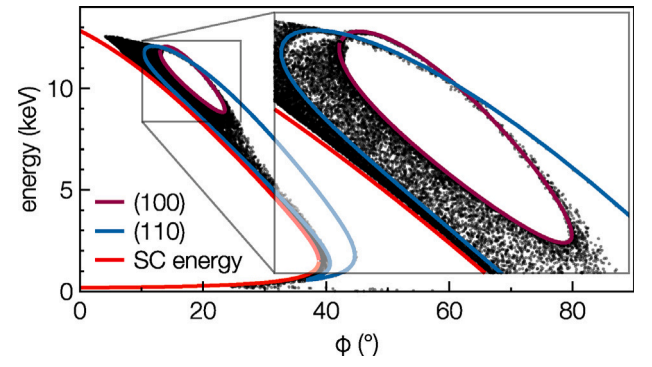

Fig. 8. Energy and angle combinations for single collisions according to Eq. (1) (grey) and for particles approaching in the (100) plane (red) as well as (110) plane (blue). The solid lines are from analytical calculations. The dots are results of a simplified MD calculation where the impact parameter is randomly chosen in both x and y direction within the unit cell of the central Mo atom at $(0, 0, 0)$. Here a 2D lattice of surface atoms was prepared. The simulated kinematics are for 14 keV Sn on Mo.

4.6. TRIM vs. Molecular dynamics

In Fig. 9 results of TRIM and LAMMPS (1900 K) calculations for $\psi = 10°$ and 14 keV are shown. For LAMMPS it becomes evident from Fig. 9(a) that the highest intensity is at higher energies than for the BCA code. This is also visible in the projected energy spectra in (g), where the high energy part of the spectrum is about twice as high for LAMMPS than for TRIM at $\phi = 15°$. This high energy shift in LAMMPS is the result of the soft multi-scattering discussed in Section 3.3 above. Also the intensity decreases faster at lower energies for LAMMPS than for TRIM. The reason is that we stopped the LAMMPS simulation at 500 fs and this underestimates ions exiting the surface later with lower energy after multiple collisions. Since we are mostly interested in the SC peak, we do not see this as a major problem. Interestingly, in (c) and (d) the 2D angular scatter pattern for LAMMPS shows a distinct structure, whereas it is almost structure-less for TRIM. For both simulations the highest intensity is around $\phi = \psi$ and decreases for larger ϕ. In (e) and (f) one can see the same angular pattern filtered for ions with energies of 10890 ± 237 eV, i.e., for an energy window where the SC peak should appear at $\phi > \psi$, i.e., outside the calculation artefact in TRIM (see discussion in Section 3.1.1). For LAMMPS, (e), there is now a more homogeneous intensity distribution for this energy window, whereas one can see two arms of intensity at around $\phi = \psi$ and $\alpha \pm 20°$. For TRIM, (f), however, one can see clearly a high intensity distribution for $\phi > \psi$ as a function of α. Indeed, the intensity distribution follows a circle in the $\alpha - \phi$ plane with a radius of 15°, which coincides with the angle ϕ at which we would expect the SC peak for the chosen energy interval (cf. Fig. 9(a)). Also here the SC peak (or better SC bow) signature vanishes for $\phi < \psi$ with only some small intensity left above the multiple scattering background (TRIM artefact). With decreasing energy the radius of the SC bow increases (not shown) as also the SC peak angle increases in (a). The angular pattern signature of the SC peak may be a way to identify it and its intensity more easily in experiment than by just observing the projected energy spectra. In (g) the projected energy spectra from LAMMPS and TRIM are shown for $\phi = (15 \pm 1)°$ and $\alpha = (0 \pm 1)°$. As discussed before, the highest energy in the spectra is 13 keV for both simulations, but LAMMPS shows a higher intensity at 12 keV than TRIM. TRIM, however, shows the SC peak prominently at around 11 keV, whereas it is absent in LAMMPS for this angle ϕ. We did additional simulations with both codes for $\psi = 5°$, 10°, and 25° and observe the same general behaviour for the SC peak in TRIM, but a clear signature of the SC peak in LAMMPS at other angles ψ as a loop in the $E - \phi$ plane, cf. Fig. 6.

4.7. Crystallinity in BCA (IMSIL)

With IMSIL we checked the importance of the crystallinity of the sample quickly for different orientations. Note that this could in principle also be done with LAMMPS but is hampered by the high computational cost of MD for many configurations. IMSIL shows a good agreement with LAMMPS (cf. Fig. 10) for the (001) surface orientation of a Mo single crystal and incidence parallel to the (100) plane with a high energy peak and sharp high energy edge. Also the spectrum falls off quickly below 10 keV for the chosen angular parameters. The experiment, however, shows a less-steep high energy edge as well as a longer tail towards lower energies. Note that the highest possible energy is lower for the aligned single-crystalline case in contrast to the poly-crystalline or amorphous ones (cf. Figs. 11 and 12, respectively).

The reason is more random multiple scattering for poly-crystalline surfaces. Also the SC peak is absent in the single-crystalline case with IMSIL, but only because the SC signature is here a loop (see inset in Fig. 10(a)) similar to the soft multi-scattering case in Fig. 8. While IMSIL does not describe true soft multi-scattering by superposition of the force fields of several atoms, it does contain a history of the trajectory at each collision due to the fixed atomic positions in a lattice. Thus, soft multi-scattering is mimicked here by a series of subsequent

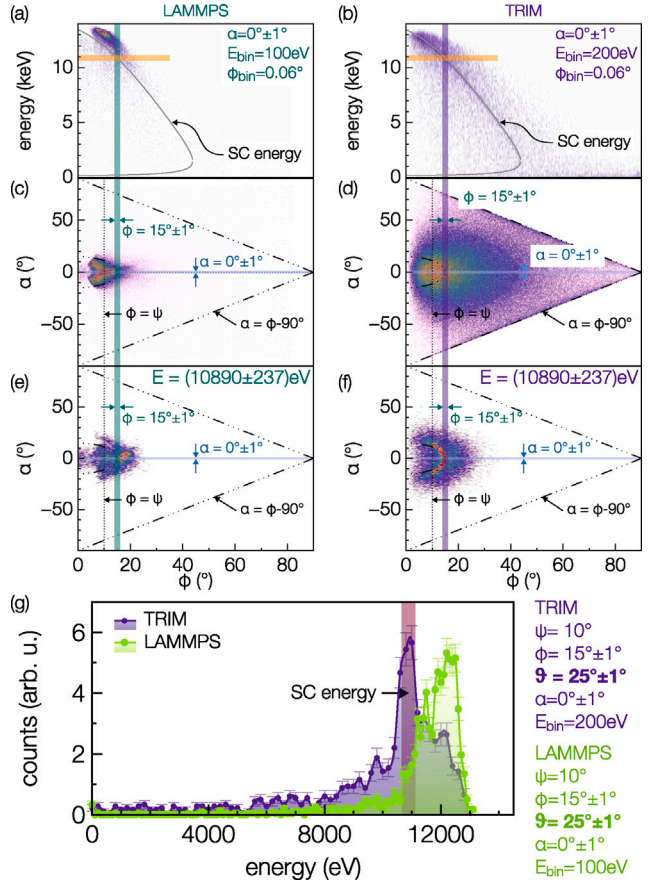

Fig. 9. Scattered ion energy and angular pattern from LAMMPS and TRIM for 14 keV Sn on Mo. (a), (c), and (e) are for LAMMPS, (b), (d), and (f) are for TRIM. (a) and (b) show the angle-dependent energy histograms with the expected SC peak energy as a grey line and the angle window used in (g) as well as energy window used in (e) and (f) marked by coloured areas. (c) and (d) show the 2D angular maps of scattered ions, where the α and Φ regions used in (g) are marked by coloured areas. (e) and (f) are the same as (c) and (d), respectively, but for ion energies between 10653 and 11127 eV, i.e., the SC peak energy range marked by a red area in (g). (g) shows the projected energy spectra for a given angular acceptance chosen as 1° for both angles.

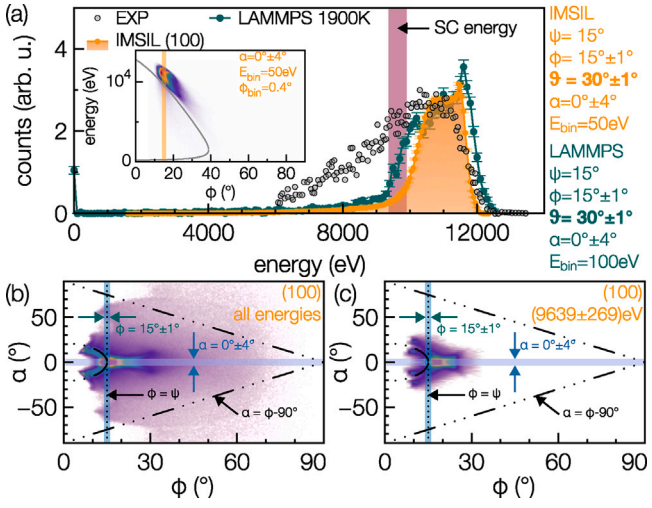

Fig. 10. IMSIL results for 14 keV Sn and a Mo single crystal a (001) surface, and with incident trajectories selected in the (100) plane (a-c) and compared to experiment and LAMMPS in (a). The angular patterns (b-c) are for all energies and for a selected energy window, respectively.

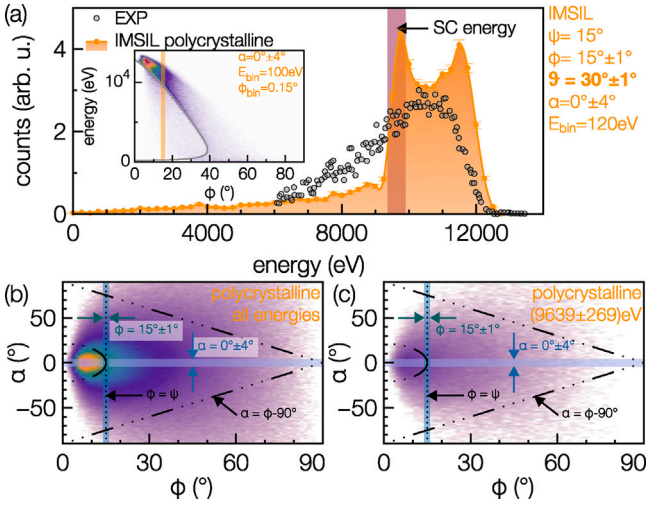

Fig. 11. IMSIL results for 14 keV Sn and a Mo single crystal (cf. Fig. 10), but the azimuthal angle of incidence is chosen randomly to mimic a poly-crystalline sample. The angular pattern (b-c) are for all energies and for a selected energy window, respectively.

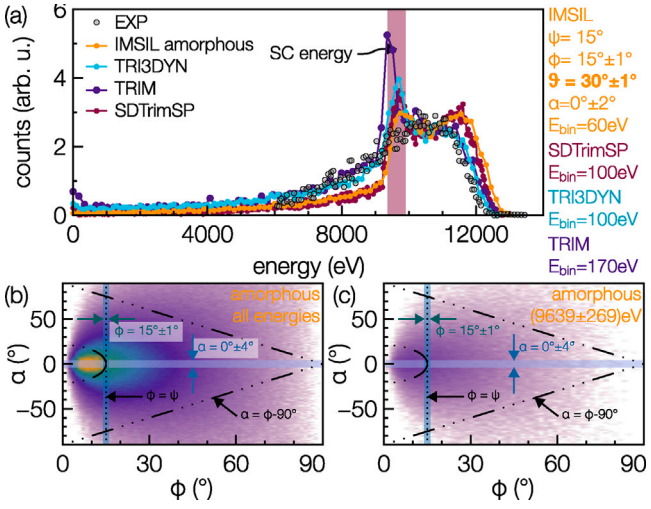

Fig. 12. IMSIL results for 14 keV Sn on Mo. The target is simulated with random atomic positions and results are compared to other BCA codes. The angular pattern (b-c) are for all energies and for a selected energy window, respectively.

binary collisions, which depend on one another. Consequently, the SC regime manifests in the loop (inset in Fig. 10(a)) and the high energy peak at 11.5 keV as well as the shoulder at 10.5 keV in Fig. 10(a). Note, that the SC peak is absent in the experiment and the shape of the spectrum is entirely different. The scattering from the single crystalline Mo surface also encodes a complex angular pattern in the $\phi - \alpha$ plane (see Fig. 10(b) and (c)).

In the poly-crystalline case (Fig. 11) the SC peak becomes clearly visible in the IMSIL simulations, again with a sharp(er) high energy edge and an edge at 9.5 keV. This spectrum is somewhat closer to the experimental one, but still with an unsatisfactory agreement. The corresponding angular pattern in Fig. 11(b) and (c) are now entirely washed out in contrast to the single crystalline case.

In Fig. 12 we simulated the amorphous case and compared the results to the other BCA codes. The angular pattern Fig. 12(b) and (c) show no structure as expected. The projected energy spectrum in Fig. 12(a) shows still an unsatisfactory agreement with the experiment for IMSIL and SDTrimSP (shown for comparison). The high energy

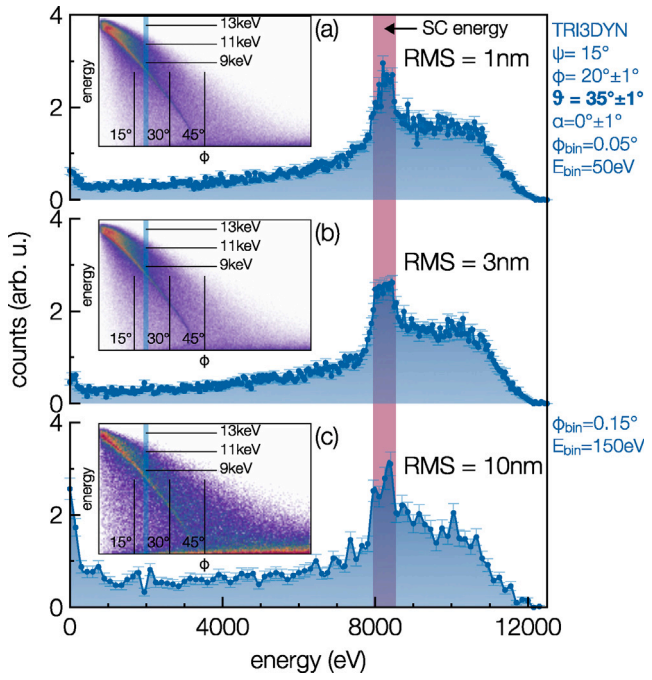

Fig. 13. Influence of the surface roughness on the backscattered ion distribution for 14 keV Sn on Mo. (a) is for a randomly generated surface with a RMS roughness of 1 nm, (b) for 3 nm and (c) for 10 nm. Note that a different binning was chosen for (c).

edge is over- and the low energy tail is under-estimated by IMSIL and SDTrimSP. TRI3DYN and TRIM, however, describe the overall shape of the experimental spectrum well. The SC peak is visible for all BCA codes, but with different intensity.

4.8. Influence of sample roughness (TRI3DYN)

TRI3DYN as the three-dimensional counterpart of TRIDYN allows the implementation of a nanostructured surface (and, if the dynamical mode is selected, to follow fluence-dependent dynamic geometrical changes). Fig. 13 shows the energy spectra for three randomly generated Mo surfaces with a pre-defined RMS roughness. Varying the RMS roughness over one order of magnitude does not significantly change the form of the spectrum. Especially the SC peak is visible for all RMS values up to 10 nm. At this largest RMS value we observe an increased intensity below 200 eV. With increasing RMS values there is an increased probability for the ions to travel inside the material before they exit. Thus, multiple scattering leading to slow backscattered ions increases.

It should be noted that TRI3DYN uses cubic voxels to describe surface roughness. While this works fine for small voxels and processes like sputtering which result from the collisional cascade typically much larger than the voxel size, a local inclination of the surface is not captured. A local surface inclination angle in combination with the effect of soft multi-scattering for a rough surface might still influence the single collision of an ion. How large this effect might be is subject to future investigation using a different description of the surface roughness and employing a specialized ray-tracing algorithm to follow ion trajectories in this particular case [22].

4.9. Influence of surface oxidation (TRI3DYN and SDTrimSP)

Mo is known to form an oxidized surface layer of the form MoO_3. Since this may have a strong effect in applications done at non-UHV conditions, we performed different TRI3DYN and SDTrimSP simulations for oxidized layers as well as adsorbate layers of CO. Fig. 14 shows TRI3DYN spectra for different CO and MoO_3 cover layers. Clearly, a cover layer of 5 Å thickness which does not contain Mo (b) leads to a completely different spectrum. As soon as Mo is contained at the surface, a SC peak is visible, but the high energy edge is significantly reduced and smeared out. This holds true for CO or O mixture with Mo. There is also no significant difference between 5 and 10 Å thickness of a MoO_3 layer, since the backscattering at these angles is very surface sensitive. Fig. 15 shows SDTrimSP calculations for a different incident angle ($\psi = 10°$) and two different oxidation states. For a low amount of oxidation ($\lesssim 10\%$) the spectrum remains similar to the pure Mo surface, even though the high energy edge and SC peak height ratios change somewhat. For full oxidation, the spectrum again changes significantly. We can draft the conclusion, that oxidation or contamination in an experiment is not a severe problem, because it would either manifest in a clear signature in the spectrum or it is so low that it does not affect the SC peak shape, position or intensity.

To put the results with SDTrimSP into context with other simulations using pure Mo, Fig. 15(a) shows in addition the TRIM and LAMMPS results for this case of angles and the pure Mo surface. SDTrimSP shows a significantly different spectral shape than both of the other codes, which is peculiar. The high energy edge is in good agreement with LAMMPS, whereas we identified this region of the spectrum in MD as a result of a soft multi-scattering. Since SDTrimSP does not consider soft multi-scattering, i.e., scattering events are independent from one another, we attribute this agreement between LAMMPS and SDTrimSP to an above-surface treatment of scattering in the latter. However, the pre-scattering is not included in TRIM, which may explain why it does not yield the same high energy edge. LAMMPS is much lower at lower energies, which again results from a cutoff in simulation time for MD. Now, TRIM is in agreement with SDTrimSP at the region below the SC peak.

4.10. Number of collisions (TRI3DYN)

In Fig. 16 we show the contribution of single, double, and multiple (i.e., more than two) collisions to the total spectrum, since TRI3DYN gives the number of collisions encountered for each backscattered ion. One can see that the single collisions (a) follow nicely the result of Eq. (1). Double collisions (b) also yield a sizeable contribution to the SC peak energy with some increased intensity above the SC ridge. This becomes clear, since backscattering with only two collisions demands two small angle scatterings. More than two collisions already yield an uniform background and no pronounced contribution to the SC peak energy.

Interestingly, the projected energy spectrum (d) for > 2 collisions is the only simulation result we obtained, which reproduces the overall experimental spectrum (cf. Fig. 17 for similar ϕ angles) and does (like the experiment) not contain a SC peak. While this might be a coincidence, we cannot unambiguously identify a reason why single and double scattering events would be missing in the experiment. Note, that the oscillatory behaviour of the TRI3DYN result in Fig. 16 is due to a re-binning and as such a minor artefact.

4.11. Comparison to experimental data

Let us now compare simulations to experimental data for various exit angles. Using $\psi = 15°$ and $\phi = 15°$, 25°, and 30° we compare to spectra obtained with an electrostatic analyser in Fig. 17(a) and (c) as well as with a time-of-flight detector in (b). All experimental spectra show no SC peak. TRIM, SDTrimSP, and TRI3DYN show a SC peak in all three spectra, whereas the case of (a) is at the intensity jump of TRIM discussed above and therefore the SC peak intensity should be considered with care. For $\phi = 30°$ in (c) the SC peak intensity in TRIM is very small. LAMMPS shows a shoulder at the expected SC

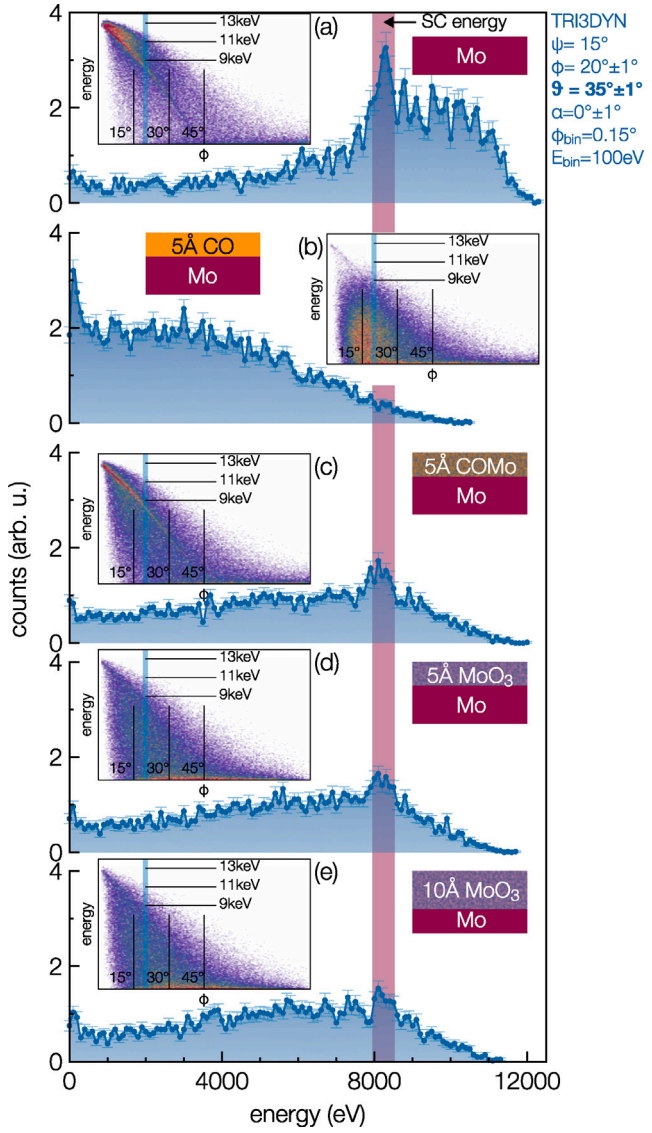

Fig. 14. Influence of surface contaminations on the backscattered ion spectrum simulated with TRI3DYN. (a) is for the pure Mo surface, (b) for a 5 Å CO cover layer, (c) for a 5 Å CO-Mo (33 at% each) cover layer, (d) for a 5 Å fully oxidized MoO_3 layer and (e) for a 10 Å MoO_3 layer.

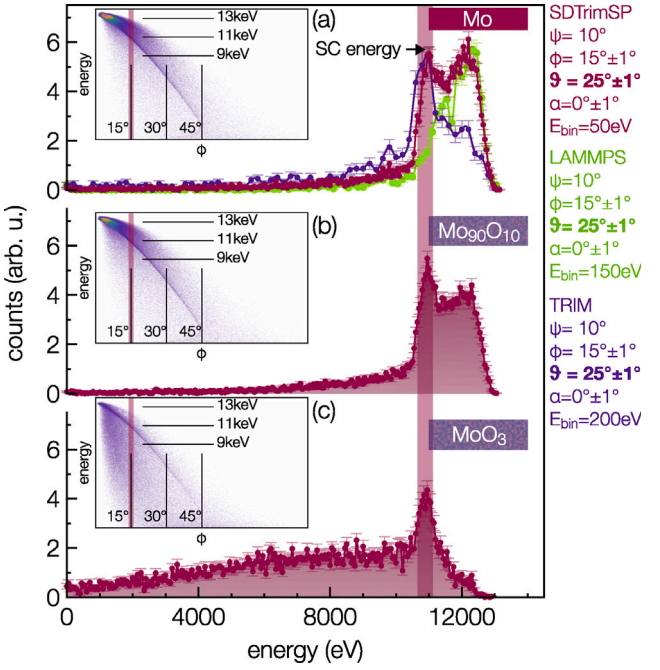

Fig. 15. Influence of surface contaminations on the backscattered ion spectrum simulated with SDTrimSP. (a) is for the pure Mo surface together with TRIM and LAMMPS calculations, (b) for a $Mo_{90}O_{10}$ layer, and (c) for a fully oxidized MoO_3 layer.

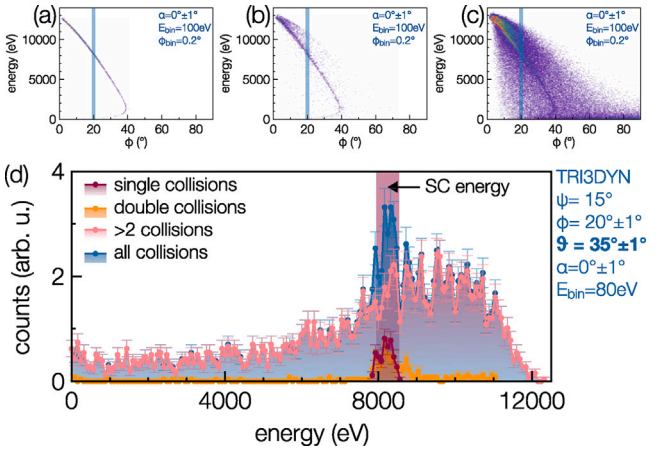

Fig. 16. TRI3DYN calculation results filtered for the number of collisions for 14 keV Sn on Mo. (a) shows the energy-angle pattern for ion which encounter only one collision, (b) for purely double collisions, and (c) for all collisions. (d) shows the projected energy spectra, where contributions to the SC peak arise from single as well as double collisions.

energy in (a) and low intensity peaks in (b) and (c). Note, that the statistics in LAMMPS is limited due to the high computational cost in contrast to BCA codes. TRI3DYN yields the best overall agreement with the experiment and the other BCA codes as well as LAMMPS show differences to the experiment at high and low energies. What remains elusive is the missing (clear) signature of the SC peak in the experiments.

From our results one can see, that the SC peak is absent in the experiment, whereas it is present in all the BCA codes and LAMMPS. For the single crystalline case of IMSIL and in LAMMPS the SC case manifests not as a single peak (or ridge in the $E-\phi$ plane), but rather in a double peak structure (i.e., a loop in the $E-\phi$ plane). Further, the scattering shows a clear angular pattern in LAMMPS and IMSIL (single crystalline) and no pattern in the other BCA codes (cf. Fig. 9(c) and (d)). An experimental spectrum at $\psi = 15°$ and $\phi = 25°$ was obtained with a time-of-flight spectrometer to collect both charged and neutral scattered particles. Note, that LAMMPS and BCA codes do not consider a charge state of the ion, i.e., particularly no charge exchange. The missing SC peak in the experiment could be explained by the fact that the charge exchange is different for a single collision than it is for multiple collisions as assumed earlier for light ions [23]. While multiple collisions involve mostly large impact parameter scattering, the single collision is connected to one comparatively small impact parameter. It was observed previously, that the charge exchange of heavy ions is very sensitive to the impact parameter [24], especially in the single scattering regime [25].

For heavy ion collisions at closer impact parameters quasi-resonant charge transfer channels might be open and the overall interaction time is shorter than for trajectories in the multiple collision regime. Further,

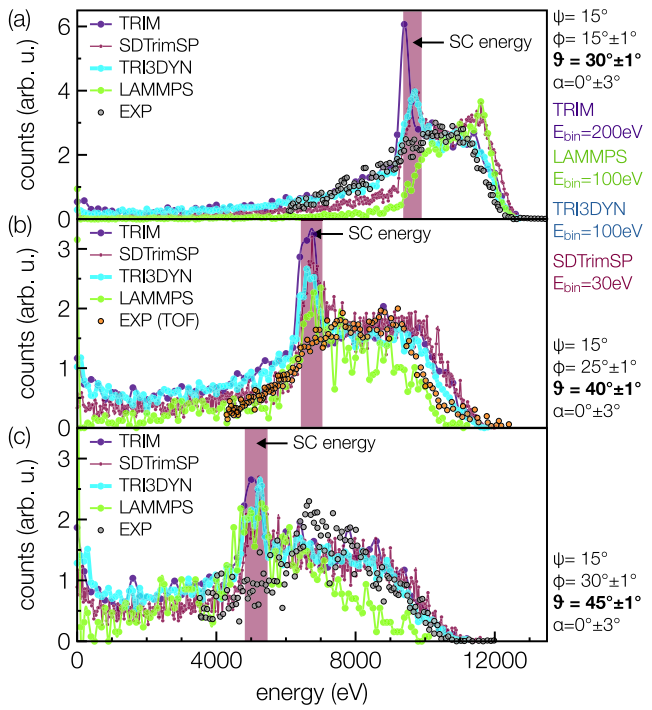

Fig. 17. Energy spectrum of 14 keV Sn on Mo for $\psi = 15°$ with experimental data obtained with an electrostatic analyser and a time-of-flight detector. (a)–(c) are for $\phi = 15°$, 25°, and 30°.

re-ionization may also occur and differ between single collision and multiple scattering trajectories. However, the time-of-flight measurement also shows no SC peak (cf. Fig. 17(b)), where neutral particles from the single collision also contribute to the signal. Unfortunately, the angle at which the spectrometer could be mounted is not ideal to look for the SC peak. We cannot exclude that the SC peak may be hidden in the experimental spectrum under these conditions due to an unfavourable position of the scattering angle and the detector acceptance angles. For all other incident angles ψ, the spectra were measured with an electrostatic analyser which only detects charged scattered ions. If neutralization is more efficient in the small impact parameter SC case, the SC peak might then be missing in these experiment.

Very recently electronic energy loss straggling was investigated in details for H and He projectiles in elemental solids [26,27]. An inhomogeneous electron density distribution in a solid is found to increase the energy straggling of heavier ions [28] significantly in comparison to straggling computed from a (homogeneous) free electron gas model. Straggling due to a fluctuating ion charge was found to have only a minor effect. This straggling due to the bunching effect of the electron density, which is not captured by BCA or MD, might lead to a significant broadening of the SC peak rendering it challenging to resolve in an experiment.

Additionally to the charge exchange another significant difference between experiment, MD and BCA exists. Molybdenum does not exist in an amorphous form, and therefore the experiment, LAMMPS, and IMSIL deal with a (poly-)crystalline surface. In crystalline surfaces one might expect an angular dependence of the scattering, which is clearly observed in LAMMPS (cf. Fig. 9(c)) and IMSIL (cf. Fig. 10). Since this angular pattern signature is strong in intensity, it may be stronger than any additional signal/pattern from the SC peak. Fig. 9(e) shows some indication for a SC peak, but it is weak compared to the intensity at other angles. The same may hold true in the experiment, where the narrow angular range of the SC peak may hide it under a strong angular dependence of the scattering yield due to the crystallinity of the surface.[1] The random media BCA codes, on the contrary, do not consider any atomic order in the surface, thus treat the Mo as amorphous. In this case the scattering distribution is homogeneous (cf. Fig. 9(d)) and the SC peak is easily visible on the homogeneous background when filtering for the correct energy (cf. Fig. 9(f)).

5. Conclusion

In conclusion, the SC peak is missing in the experiment and the reason might be either the crystalline nature of the surface introducing an additional angular pattern on the scattering apart from the expected one for the SC peak; or charge exchange of the ions is strongly different between the single collision and the multiple collision regime at the same final scattering angles and energies. From the simulations at hand and the experiments here, we cannot unambiguously identify the main reason for the missing SC peak, but we can make suggestions for future experiments. In these, energy- and angle-resolved scatter patterns should be collected over the large range of 20° with and without neutral particles contributing to a spectrum. Covering a large angular range would allow to discern a large fraction of the angular pattern (for example, cf. Fig. 10(b) or (c)) instead of just a single angular projection of the energy spectrum.

Possible influences on the SC peak in the experiment arising from surface oxidation or sample roughness were checked with TRI3DYN and SDTrimSP. Even 10 nm RMS roughness (see Appendix) could not explain the missing SC peak and both oxidation of Mo and coverage of the surface with light contaminations (CO) would shift the high energy edge significantly. We therefore conclude, that the experimental data is not influenced significantly by oxidation or contamination.

As another result we emphasize, that TRIM shows a severe artefact for backscattered ions at $\phi < \psi$, which needs to be carefully considered when using TRIM. LAMMPS, however, can be used to simulate the experimental spectra also with some discrepancies at higher energies and a low-energy cutoff due to a limited simulation time. In general, high statistics are needed in simulations to filter all scattered ions for a particular 2D angular range and energy interval. This limits the applicability of molecular dynamics.

TRIDYN, TRI3DYN, IMSIL and SDTrimSP are clearly favourable over TRIM since they do not show any artefact in the extracted data, allow more access to the data of the backscattered ions, are actively maintained and further developed, allow changing of interaction potentials, numerical calculation methods and electronic stopping models. All this is important to compare to an experiment and to identify sources of discrepancies if they appear. With a newly developed and freely available GUI for SDTrimSP [29] and TRIDYN [30] we are confident that these codes will be used more frequently by many users in the future. One note of caution should be given when using BCA codes for near-surface scattering, because the use of an ASL in the simulations may or may not be justified and in our particular case it obscures the result leading to a worse agreement with experiment.

Having multiple sophisticated simulation methods at hand, we are still not able to fully describe experimental findings in a relatively simple experimental scheme for single scattering of ions at surfaces. This lack of predictability of simulations and even post-fact descriptions of experiments clearly shows that additional research is needed in the field of ion-solid interaction, in particular for projectile ions heavier than H or He.

[1] We highlighted the calculated position of the SC signal in the $\alpha - \phi$ plane in each respective graph by a dashed-dotted line.

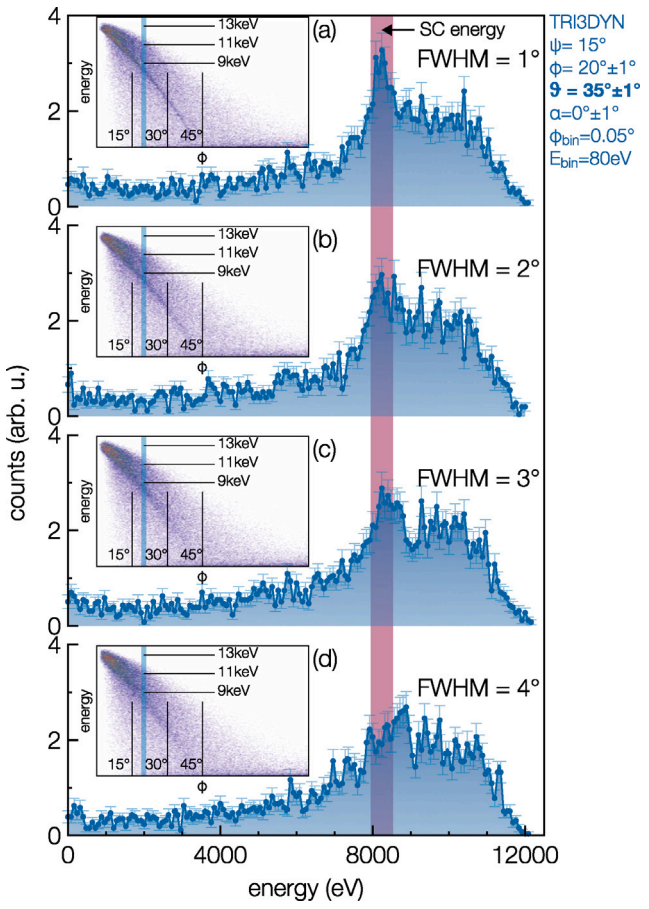

Fig. 18. Energy spectra for 14 keV Sn on Mo from TRI3DYN using a Gaussian angular distribution of the incident angle with a FWHM of (a) 1°, (b) 2°, (c) 3°, and (d) 4°. The insets show the full energy-angle 2D histogram where the SC ridge becomes less visible for larger FWHM. The coloured areas in the insets are the angular range used for extracting the energy spectra.

CRediT authorship contribution statement

R.A. Wilhelm: Wrote the manuscript, Performed the TRIM SIMULATIONS. **M.J. Deuzeman:** Performed the experiment. **S. Rai:** Performed the experiment. **W. Husinsky:** Performed the LAMMPS simulation. **P.S. Szabo:** Performed the SDTrimSP simulations. **H. Biber:** Performed the SDTrimSP simulations. **R. Stadlmayr:** Performed the TRI3DYN simulations. **C. Cupak:** Performed the SDTrimSP simulations. **J. Hundsbichler:** Performed the simplifed MD simulations. **C. Lemell:** Performed the simplifed MD simulations. **W. Möller:** Performed the TRIDYN simulations. **A. Mutzke:** Advised for the SDTrimSP simulations. **G. Hobler:** Performed the IMSIL simulations. **O.O. Versolato:** Conceptual planning of the experiment. **F. Aumayr:** Worked on the manuscript and advised work on the BCA simulations. **R. Hoekstra:** Conceptual planning of the experiment.

Data availability

Data will be made available on request.

Acknowledgements

This work was funded by the Austrian Science Fund FWF (Project No. Y 1174-N36, I 4914-N, and I 4101-N36). Financial support has also been provided by KKKÖ (commission for the coordination of fusion research in Austria at the Austrian Academy of Sciences - ÖAW). We thank S. Höfinger (VSC Research Center, TU Wien) for help with the LAMMPS simulations. Computational results pertaining to LAMMPS have been achieved using the Vienna Scientific Cluster.

Appendix

In order to assess the importance of other beam and sample parameters for the observation of the SC peak, we used SDTrimSP, TRIDYN and TRI3DYN as they allow access to these parameters in contrast to TRIM. In Fig. 18 one can see the energy spectra of the Sn beam from a flat Mo surface with 4 different angular widths of the incident beam. We used a Gaussian shaped angular distribution of the incoming ions with a full-width-at-half-maximum (FWHM) of 1–4°. With increasing FWHM the SC peak smears out and almost vanishes for 4°. Note, that the FWHM amounts to < 1° in the experiment. Although obvious, this is the symmetric case to increasing the acceptance angle of a detector, i.e., increasing the angular bin widths $\delta\alpha$ and $\delta\phi$. Interestingly, the SC peak position moves to slightly higher energies with increasing FWHM.

References

[1] M. Purvis, I.V. Fomenkov, A.A. Schafgans, M. Vargas, S. Rich, Y. Tao, S.I. Rokitski, M. Mulder, E. Buurman, M. Kats, J. Stewart, A.D. LaForge, C. Rajyaguru, G. Vaschenko, A.I. Ershov, R.J. Rafac, M. Abraham, D.C. Brandt, D.J. Brown, Industrialization of a robust EUV source for high-volume manufacturing and power scaling beyond 250W, in: Extreme Ultraviolet (EUV) Lithography IX, Vol. 10583, SPIE, 2018, 1058327.
[2] O.O. Versolato, Physics of laser-driven tin plasma sources of EUV radiation for nanolithography, Plasma Sources. Sci. Technol. 28 (8) (2019) 083001.
[3] V.Y. Banine, K.N. Koshelev, G.H.P.M. Swinkels, Physical processes in EUV sources for microlithography, J. Phys. D: Appl. Phys. 44 (25) (2011) 253001.
[4] J. Benschop, V. Banine, S. Lok, E. Loopstra, Extreme ultraviolet lithography: Status and prospects, J. Vac. Sci. Technol. B 26 (6) (2008) 2204.
[5] F. Torretti, J. Sheil, R. Schupp, M.M. Basko, M. Bayraktar, R.A. Meijer, S. Witte, W. Ubachs, R. Hoekstra, O.O. Versolato, A.J. Neukirch, J. Colgan, Prominent radiative contributions from multiply-excited states in laser-produced tin plasma for nanolithography, Nature Commun. 11 (1) (2020) 2334.
[6] M. Murakami, Y. Kang, K. Nishihara, S. Fujioka, H. Nishimura, Ion energy spectrum of expanding laser-plasma with limited mass, Phys. Plasmas 12 (2005) 062706.
[7] A.Z. Giovannini, N. Gambino, B. Rollinger, R.S. Abhari, Angular ion species distribution in droplet-based laser-produced plasmas, J. Appl. Phys. 117 (3) (2015) 033302.
[8] A. Bayerle, M.J. Deuzeman, S. van der Heijden, D. Kurilovich, T. de Faria Pinto, A. Stodolna, S. Witte, K.S.E. Eikema, W. Ubachs, R. Hoekstra, O.O. Versolato, Sn ion energy distributions of ns- and ps-laser produced plasmas, Plasma Sources. Sci. Technol. 27 (4) (2018) 045001.
[9] D.J. Hemminga, L. Poirier, M.M. Basko, R. Hoekstra, W. Ubachs, O.O. Versolato, J. Sheil, High-energy ions from Nd: YAG laser ablation of tin microdroplets: comparison between experiment and a single-fluid hydrodynamic model, Plasma Sources. Sci. Technol. 30 (10) (2021) 105006.
[10] Q. Huang, V. Medvedev, R. van de Kruijs, A. Yakshin, E. Louis, F. Bijkerk, Spectral tailoring of nanoscale EUV and soft x-ray multilayer optics, Appl. Phys. Rev. 4 (1) (2017) 011104.
[11] J.F. Ziegler, M. Ziegler, J. Biersack, SRIM – The stopping and range of ions in matter (2010), Nucl. Instrum. Methods Phys. Res. B 268 (11–12) (2010) 1818–1823.
[12] W. Möller, W. Eckstein, Tridyn — A TRIM simulation code including dynamic composition changes, Nucl. Instrum. Methods Phys. Res. B 2 (1–3) (1984) 814–818.
[13] W. Möller, TRI3DYN - Collisional computer simulation of the dynamic evolution of 3-dimensional nanostructures under ion irradiation, Nucl. Instrum. Methods Phys. Res. B 322 (2014) 23–33.
[14] A. Mutzke, R. Schneider, W. Eckstein, R. Dohmen, SDTrimSP Version 5.00, IPP-report 12/8 (2011) 1–70.
[15] G. Hobler, Monte Carlo simulation of two-dimensional implanted dopant distributions at mask edges, Nucl. Instrum. Methods Phys. Res. B 96 (1–2) (1995) 155–162.
[16] https://www.lammps.org.
[17] S. Plimpton, B. Hendrickson, A new parallel method for molecular dynamics simulation of macromolecular systems, J. Comput. Chem. 17 (3) (1996) 326–337.
[18] A.P. Thompson, H.M. Aktulga, R. Berger, D.S. Bolintineanu, W.M. Brown, P.S. Crozier, P.J. in 't Veld, A. Kohlmeyer, S.G. Moore, T.D. Nguyen, R. Shan, M.J. Stevens, J. Tranchida, C. Trott, S.J. Plimpton, LAMMPS - A flexible simulation tool for particle-based materials modeling at the atomic, meso, and continuum scales, Comput. Phys. Comm. 271 (2022) 108171.

[19] M.J. Deuzeman, Generation and Interactions of Energetic Tin Ions (Ph.D. thesis), Rijksuniversiteit Groningen, Groningen, 2019, OCLC: 1103313127.
[20] S. Rai, K. Bijlsma, S. Koeleman, O. Tjepkema, A. Noordam, H. Jonkman, O. Versolato, R. Hoekstra, Single-Collision scattering of keV-energy Kr ions off a polycrystalline Cu surface, Nucl. Instrum. Methods Phys. Res. B 482 (2020) 58–63.
[21] W. Möller, Private correspondance.
[22] C. Cupak, P. Szabo, H. Biber, R. Stadlmayr, C. Grave, M. Fellinger, J. Brötzner, R. Wilhelm, W. Möller, A. Mutzke, M. Moro, F. Aumayr, Sputter yields of rough surfaces: Importance of the mean surface inclination angle from nano- to microscopic rough regimes, Appl. Surface Sci. 570 (2021) 151204.
[23] D. Primetzhofer, S. Rund, D. Roth, D. Goebl, P. Bauer, Electronic excitations of slow ions in a free electron gas metal: Evidence for charge exchange effects, Phys. Rev. Lett. 107 (16) (2011) 163201.
[24] R.A. Wilhelm, E. Gruber, R. Ritter, R. Heller, S. Facsko, F. Aumayr, Charge exchange and energy loss of slow highly charged ions in 1 nm thick carbon nanomembranes, Phys. Rev. Lett. 112 (15) (2014) 153201.
[25] S. Creutzburg, A. Niggas, D. Weichselbaum, P.L. Grande, F. Aumayr, R.A. Wilhelm, Angle-dependent charge exchange and energy loss of slow highly charged ions in freestanding graphene, Phys. Rev. A 104 (4) (2021) 042806.
[26] F. Selau, H. Trombini, R. Fadanelli, M. Vos, P. Grande, On the energy-loss straggling of protons in elemental solids: The importance of electron bunching, Nucl. Instrum. Methods Phys. Res. B 497 (2021) 70–77.
[27] F. Selau, A. Molling, H. Trombini, R. Fadanelli, M. Vos, P. Grande, Energy-loss straggling of helium in elemental solids: The importance of the charge-exchange and bunching effects, Thin Solid Films 783 (2023) 140038.
[28] S. Lohmann, R. Holeňák, P.L. Grande, D. Primetzhofer, Trajectory dependence of electronic energy-loss straggling at keV ion energies, Phys. Rev. B 107 (8) (2023) 085110.
[29] P. Szabo, D. Weichselbaum, H. Biber, C. Cupak, A. Mutzke, R. Wilhelm, F. Aumayr, Graphical user interface for SDTrimSP to simulate sputtering, ion implantation and the dynamic effects of ion irradiation, Nucl. Instrum. Methods Phys. Res. B 522 (2022) 47–53.
[30] A. Redl, BCA-Guide, TU Wien, https://github.com/atomicplasmaphysics/BCA-Guide.